Master's Thesis of Engineering

Controllable Actuation of Magnetic Kirigami Patterns

자성 키리가미 패턴 구조의 동작 제어 연구

August 2019

Graduate School of Engineering
Seoul National University
Materials Science and Engineering Major

Trivoramai Jiralerspong

Controllable Actuation of Magnetic Kirigami Patterns

지도교수 김 상 국

이 논문을 공학석사 학위논문으로 제출함
2019년 08월

서울대학교 대학원
공과대학 재료공학부
Trivoramai Jiralerspong

Trivoramai Jiralerspong의 공학석사
학위논문을 인준함
2019년 08월

위 원 장 홍 성 현 (인)

부위원장 김 상 국 (인)

위 원 강 승 균 (인)

Abstract

Controllable Actuation of Magnetic Kirigami Patterns

Trivoramai Jiralerspong
Department of Materials Science and Engineering
The Graduate School
Seoul National University

The art of paper cutting, kirigami, and its shape transformation capabilities have shown remarkable advancements in the field of science and engineering. A kirigami pattern consists of cuts that are made on a single sheet of material, where planar mechanical deformations could induce shape transformations in both two-dimensional (2D) and three-dimensional (3D). Due to this remarkable property, kirigami patterns could give rise to complex material properties such as auxetics and mechanical metamaterials where they expand when subjected planar deformations. However, the mechanical deformations of kirigami structures are usually performed physically by hand or machine, and therefore limiting its application in small and tight spaces where access is difficult. To counter this problem, this study proposes a remote control technique of kirigami patterns using

magnetic fields as an external stimulus.

In this work, the remote control of kirigami patterns in 2D and 3D is demonstrated by programming the magnetic anisotropy of magnetic nanoparticle (MNP) chains within the magnetic-elastomer composite. The kirigami patterns considered consists of multiple square units that are connected by hinges. Various 2D and 3D shape transformations are produced by changing the magnetic anisotropy within each square unit and the placement of the hinges. The fabrication and the experimental procedures are performed under a uniform magnetic field that is generated by an electromagnet. Experimental results demonstrate that by aligning the MNP chains within each square unit in-plane and out-of-plane, 2D and 3D shape transformation can be achieved. Hence, the validity of the proposed technique that uses magnetic fields to control magnetic anisotropic kirigami patterns are confirmed. This untethered actuation of kirigami patterns show promising potential applications in areas such as drug delivery, medical patches, and artificial valves.

Keywords: kirigami, soft actuator, magnetic anisotropy programming, chained magnetic nanoparticles, 2D actuation, 3D actuation.

Student Number: 2017-22386

Table of Contents

List of Figures

List of Tables

Chapter 1. Introduction

Chapter 1 introduces the research through three different sections. Section 1.1 states the motivation of the research. Section 1.2 describes the aim and approach to the research. Section 1.3 provides an overview of the layout of the thesis.

1.1. Motivation

Kirigami is a Japanese and Chinese art of paper cutting which involves the cutting of a single thin sheet of material into patterns. These patterns have the ability to transform from one shape to another and revert back to its original form. By performing planar mechanical deformations, it can induce shape transformations in both 2D and 3D. However, one of the drawbacks of the existing kirigami patterns is that the planar deformations are usually performed physically by hand or machine. This limits the ability of the kirigami patterns to achieve shape transformation in small and tight spaces where direct contact is difficult. Furthermore, since extra equipment and human labor is required to bring about the planar deformations of the kirigami patterns, it causes the actuating system to be complex, inconvenient, and costly, as extra components are required to actuate the shape. To

counter this problem, remote actuation through an external stimulus is introduced as means to control the shape transformation of kirigami patterns in 2D and 3D, without direct contact with the shape. The remote control of kirigami patterns, specifically by using the magnetic field, has yet to be studied.

1.2. Research Aims and Approach

This study aims to explore on the remote actuation of kirigami patterns by means of the magnetic field as an external stimulus to bring about shape transformation in 2D and 3D. To realize this aim, the kirigami patterns are fabricated using a magnetic-elastomer composite, that are able to provide controllable magnetic actuation, due to the magnetic anisotropy introduced by the magnetic nanoparticle (MNP) chains. This work attempts to achieve shape morphologies in both 2D and 3D by reconfiguring the MNP chain orientation in- and out-of-plane. The 2D and 3D actuation are demonstrated by using simple kirigami designs comprised of square units that are connected by hinges. In addition, different variations in cut designs, size and experimental conditions of the kirigami patterns are explored. Finally, the actuation performance of these patterns and its magnetic properties are evaluated.

1.3. Organization of the Thesis

The thesis is organized as follows:

Chapter 2 presents the background and overview of the kirigami patterns, remote actuation of soft materials, and magnetic actuation of magnetic soft materials.

Chapter 3 proposes the design principle of the kirigami patterns used in this study. The concept and the method used to program the magnetic anisotropy will be discussed. A mathematical model will also be introduced to further explain the 2D and 3D actuation of kirigami patterns.

Chapter 4 offers a detailed explanation on the design and the fabrication method of the magnetic kirigami patterns. Schematic illustrations of the embedded chains within the square units of each kirigami pattern design, as well as the actuated profiles of the kirigami patterns are shown.

Chapter 5 presents the experimental design, conditions, setup, and procedure conducted in this study. Five different experiments are performed to confirm the 2D and 3D magnetic actuation of kirigami patterns.

Chapter 6 provides the results of the all the five experiments conducted in this study. The results obtained are compared with the proposed mathematical model. The magnetic properties of the kirigami

patterns are measured using the vibrating sample magnetometer (VSM) and characterized with an optical microscope.

Chapter 7 discusses about the findings and the results obtained. The limitations of the fabrication method and the actuation of the kirigami patterns will be emphasized.

Chapter 8 concludes the thesis. The obtained results are summarized and discussed in this chapter. In addition, the contributions and future work will also be highlighted.

Chapter 2. Background and Overview

Chapter 2 offers background information about kirigami patterns and its shape transformation capabilities. Remote actuation of soft materials using external stimuli are introduced as means to actuate the kirigami pattern. Emphasis will be put upon magnetic actuation, as magnetic fields offer the best mode of control.

2.1. Kirigami Patterns

Kirigami (切り紙), is an ancient paper (-gami 紙) cutting (kiri-切り) art form where cuts are made on a single sheet of material. Through different cut patterns and planar deformations, kirigami patterns could give rise to shape transformation in both 2D and 3D, depending on the cut designs [1]–[6]. This property of kirigami patterns give rise to conventional and unconventional material properties [6]–[11], as shown in Figure 1.

Conventional everyday materials (Figure 1 (a)) exhibit a positive Poisson's ratio, where the materials expand (contract) along the axial tensile (compressive) load [9]. For example, when stretching a rubber band, the length becomes longer along the direction that it is stretched, and narrower in the cross section. On the other hand, unconventional

materials (Figure 1 (b) and (c)) such as mechanical metamaterials and auxetic materials, possess zero or negative Poisson's ratio [9], [10]. Materials with zero Poisson's ratio has no transverse deformations upon axial loading, such as wine bottle corks [12]. Materials with negative Poisson's ratio however, expand when subjected to tensile loading and compressed upon compressive loading, such as a special designed foam [13] and chiral honeycomb structures [14].

Kirigami patterns are not limited only to rigid materials such as paper, but are also applicable to flexible and soft materials such as polymers and elastomers [15]–[21]. These materials possess elastic properties that allow kirigami patterns to revert back to its original structure after subjected to planar deformations [22]–[25]. Due to this reason, kirigami patterns could induce intriguing material properties to planar materials, bringing about promising potential applications in solar cells [26], foldable batteries [27], flexible electronics [28], and even medical bandages [15].

Although kirigami patterns are widely studied in the field of science and engineering, and have demonstrated a wide range of applications, one of the disadvantages is its actuation method. Kirigami patterns rely on the human hand or mechanical testing systems in which direct contact with the shape is necessary to perform the shape transformation [29]–[32]. This causes the actuating system to be

complex, inconvenient, and costly. Due to this reason, the actuation of kirigami patterns are limited to only large areas, i.e. the actuation of kirigami patterns in small and tight spaces, such as in the human body, is impossible. For instance, Dias et al. [29] demonstrated the morphology of kirigami patterns on a thin elastic sheet, where cuts are patterned and deformed by a mechanical testing system, Instron 5943. Similarly, Cho et al. [20] demonstrated the application of elastic kirigami fractal cut patterns by stretching the pattern mechanically by hand and have demonstrated its use as a stretchable electrode. Likewise, the afore mentioned applications of kirigami patterns [15], [26], [28], all require physical contact to perform the deformations. In particular, Morikawa et al. [28] demonstrated the practical use of kirigami as a microelectrode device that is used to record in vivo biosignals. However, an open surgery must be performed in order to physically place the stretched electrode at the targeted area. To tackle this problem, remote control through external stimuli can be used to control the shape transformation of kirigami patterns, where direct contact of the shape can be avoided.

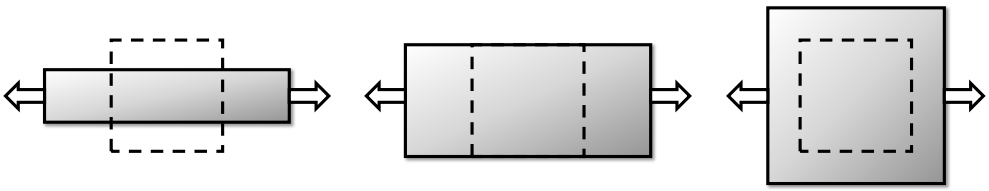

(a) (b) (c)

Figure 1. Conventional and unconventional material properties of subjected to tensile loading, demonstrating (a) positive, (b) zero, and (c) negative Poisson's ratio.

2.2. Remote Actuation

Remote actuation of an object is performed by means of an external stimulus such as light [33], [34], heat [35], solvent [36], and magnetic fields [37]–[41], where the object's material respond to the applied stimuli. Reconfigurable stimuli-responsive soft polymeric materials in particular, offer reversible properties, as its shape is able to revert back to its original structure upon removal of the external stimuli [18], [22], [42]. Each stimulus and its stimuli-responsive material offer its own advantages and disadvantages. One of the significant disadvantages of utilizing an external stimulus such as solvent, is its slow response time, as it requires a certain amount of time for the object to reach its final actuated shape [36]. However, materials that offer a fast response to the external stimuli, such as light- and heat-responsive materials, suffer biocompatibility issues,

as the tissues surrounding the material are damaged upon the application of the stimulus [42]. Magnetic fields on the other hand, counters these issues, as it provides a fast, safe, biologically friendly, and effective control [38], [40], [43].

2.3. Magnetic Actuation

Actuation of soft materials by means of a magnetic field as an external stimulus requires a material that can respond to the applied magnetic field. Examples of magnetically responsive soft materials include magnetorheological elastomers and ferrogels [44], [45]. Magnetorheological elastomers (MREs) is a type of magnetorheological materials (MR), which is a class of smart materials that have rheological properties that respond rapidly upon the application of an external magnetic field [44]. MREs is a mixture of two components: the magnetic particles and the polymer matrix.

The magnetic (ferromagnetic) particles used in MREs are either magnetically-hard particles such as neodymium-iron-boron (NdFeB), or magnetically-soft particles such as iron and iron oxides. The main difference between the hard or soft magnetic particles is the coercivity of the particles. Magnetically-hard particles have high coercivity and can retain high remnant magnetization, as long as they are magnetically saturated [45]. Recent studies have demonstrated

promising applications of hard-magnetic particles in MREs in soft robotics, as they can perform complex shape transformation [38]–[40]. Hu et al. [40] proposed a novel soft bodied robot with high mobility that can walk, roll, jump, climb, and swim in both wet and dry environments. Similarly, Kim et al. [38] developed a fabrication technique that can 3D print programmable domains of hard-magnetic soft materials. However, the drawback of using hard-magnetic particles is its biocompatibility, which is a crucial factor that inhibit its biomedical application, as direct contact of the particles can harm biological tissues. Even though several studies [39], [40] have proposed the encasement of the MREs with a layer of biocompatible polymer, issues relating to particle leakage and durability have not been addressed. Furthermore, to saturate the hard-magnetic particles, a large magnetic field (approximately 1.6 T for NdFeB) is required. Magnetically-soft particles on the other hand, can counter these issues. Soft magnetic particles, particularly Fe_3O_4 iron oxide nanoparticles, is biocompatible and has been approved by the Food and Drug Administration (FDA) [46]–[49]. In addition, magnetically soft-magnetic particles do not require a large magnetic field, as they have low coercivity and cannot retain remnant magnetism once the applied magnetic field is removed [49]. Even though soft magnetic particles can develop strong magnetization when the magnetic field is

applied [45], when used as part of MREs to fabricate actuators and robots, the shape transformation abilities and its control is inferior to that of hard magnetic particles. However, the control can be enhanced by functionalizing the MRE to have magnetic anisotropic properties [37], [44], [50], [51].

The second component of the MRE, the polymer matrix, plays an important role in functionalizing the material. Due to the nature of the polymer matrix that is able to crosslink, the material exists in two states: the cured and the uncured states. The MREs that is initially uncured allow magnetic particles to evenly distribute throughout the polymer matrix, which makes the material isotropic. Prior to curing of the MRE, the rheological properties can be changed under the influence of the magnetic field [44], since the MNPs are allowed to move through the polymer matrix to self-assemble into chains by dipolar interactions [51]. Each MNPs are pulled towards each other, in a head-to-tail manner along the direction of the applied uniform magnetic field, as shown in Figure 2. Over time, the polymer matrix crosslinks and cures, and embeds the MNP chains permanently within the matrix. Functionalizing the MRE this way brings about anisotropic magnetic properties to the material. Magnetic anisotropic materials respond to the external magnetic field by aligning the embedded chains to the direction of the applied field. Upon removal of the field, the

functionalized MREs are able to revert back to its original shape without damage, due to the elastic properties of the polymer matrix [18], [22]. In this research, the MRE is fabricated using iron oxide (Fe_3O_4) nanoparticles and silicone elastomer, and is termed 'magnetic-elastomer composite'.

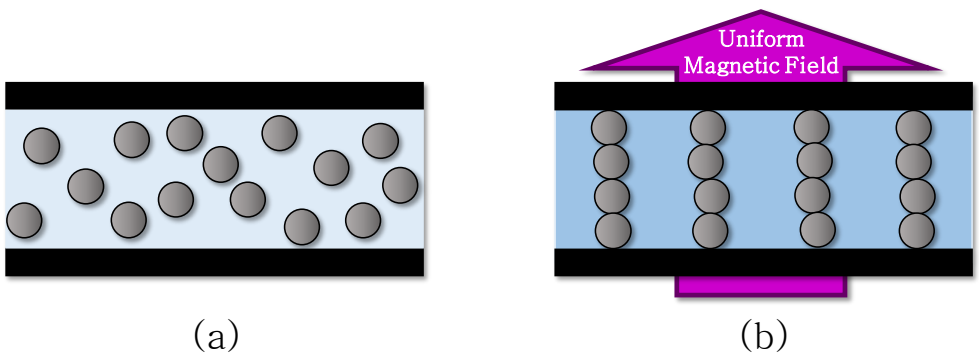

Figure 2. The behavior of the magnetorheological elastomer (a) before and (b) after the application of an external uniform magnetic field. The MNPs are uniformly distributed in (a), and form chains in (b).

Chapter 3. Modelling

Chapter 3 starts by introducing the design and actuation principle of the kirigami patterns. The concept of magnetic anisotropy and the method of programming the magnetic anisotropy is described later on in this chapter, before discussing about the mathematical model of the 2D and 3D actuation of kirigami patterns.

3.1. Design Principle

The design of the kirigami patterns mainly consists of square units and hinges. Each square units are separated by horizontal and vertical 'cuts' i.e. space, and are joined together by hinges at the vertices to form a single sheet of material, as illustrated in Figure 3.

The shape transformation of the kirigami patterns is mainly caused by the square units that move independently of each other. They are fabricated using the magnetic-elastomer composite, that is functionalized to give the material magnetic anisotropy. The morphology of the actuated kirigami shape can be designed by considering the direction of the MNP chains within each square unit with respect to the actuating magnetic field. The hinges on the other hand, are fabricated using only the silicone elastomer. Since the hinges

join the square units together, they aid in the movement of the kirigami patterns and prevent the deformation of the square units during shape transformation. In other words, upon application of an external magnetic field, the movement of the square units causes the connected hinges to bend. Therefore, by designing the 'cuts', i.e. the placement of the hinges within the kirigami patterns, as well as the magnetic anisotropy within each square unit, unique shape transformation of kirigami patterns can be achieved.

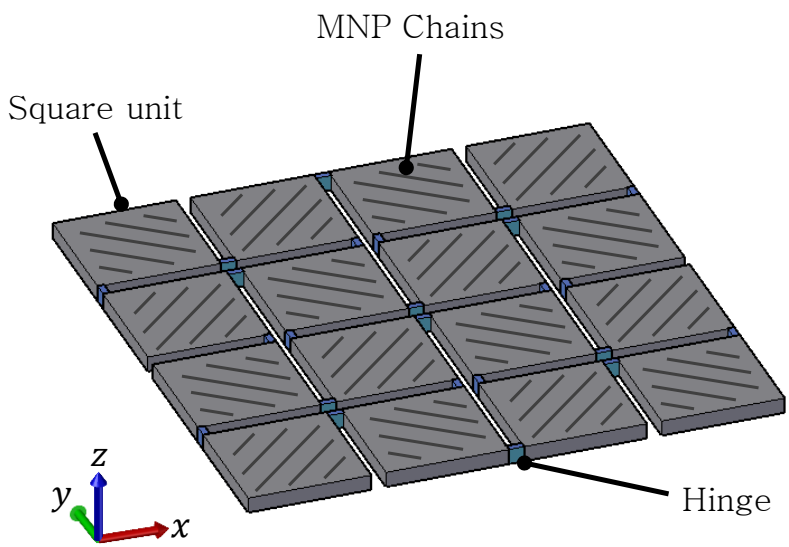

Figure 3. Kirigami pattern design composed of square units that are connected by hinges. The square units are functionalized to have magnetic anisotropic properties. The spaces between the hinges illustrate the 'cuts' of the kirigami patterns.

3.2. Programming the Magnetic Anisotropy

Anisotropic materials have their own directionality, and so does magnetic anisotropic materials. Materials with magnetic anisotropic properties respond immediately to an applied external uniform magnetic field to align its magnetic moment along the direction of applied magnetic field, as it is the most energetically favorable orientation. Therefore, the square units of the kirigami patterns that are fabricated from the functionalized magnetic-elastomer composite too, can respond quickly to the applied magnetic field. This is due to the fact that the embedded MNP chains within each square unit can turn to align itself along the direction of the applied magnetic field. In other words, the angle which the chains make with the applied field will determine the motion of the square units and hence the kirigami shape as a whole.

The magnetic anisotropy of each square unit within the kirigami pattern can be programmed individually. This is due to the nature of the magnetic-elastomer composite that can exist in two states: the uncured and cured states. Prior to the composite being cured, the composite exists as an isotropic material, since the magnetic particles are evenly distributed throughout the polymer matrix. With the application of the external magnetic field, the MNPs are allowed to move and self-assemble to align into chains along the direction of the

field. Once the elastomer is cured, the chains are fixed within the composite, even after the removal of the field, giving the composite anisotropic magnetic characteristics. Furthermore, since the uncured matrix is in liquid phase, and cures to become a solid, the composite can take up any shape.

In this study, the applied uniform magnetic field, B_x, used to align the MNPs and to actuate the kirigami patterns is defined to be in the x-direction. The 2D and 3D shape transformation of the kirigami pattern depends on the orientation of the chains within the 3D space, relative to the direction of the applied B_x, as shown in Figure 4 (a). To achieve shape transformation in 2D, the chains within each square unit must be oriented 'in-plane', along the xy-plane, at an angle of θ_{xy} with respect to B_x. As shown in Figure 4 (b), the chains are formed along the surface of the square units. Similarly, to achieve shape transformation in 3D, the chains within each square unit must be oriented 'out-of-plane', along the xz-plane, at an angle of θ_{xz} with respect to B_x. The chains are therefore formed along the thickness of the square units, as illustrated in Figure 4 (c). It is to be noted that gravity is acting along the z-axis.

To program the magnetic anisotropy, the functionalized square units of different chain orientation are assembled in the 2D plane (xy-plane), to form a complete kirigami pattern, as shown in Figure 4 (b)

and (c). In other words, the assembly of the square units that are functionalized 'in-plane', can bring about 2D actuation of the kirigami patterns, where the original 2D pattern transforms into a new 2D pattern. Likewise, the assembly of the square units that are functionalized 'out-of-plane', can bring about the shape transformation from the original 2D pattern to a new 3D pattern. Hence, through programming the magnetic anisotropy, the morphology of the kirigami patterns, that are originally 2D, can be controlled to actuate in any direction, depending on the direction of the MNP chains programmed.

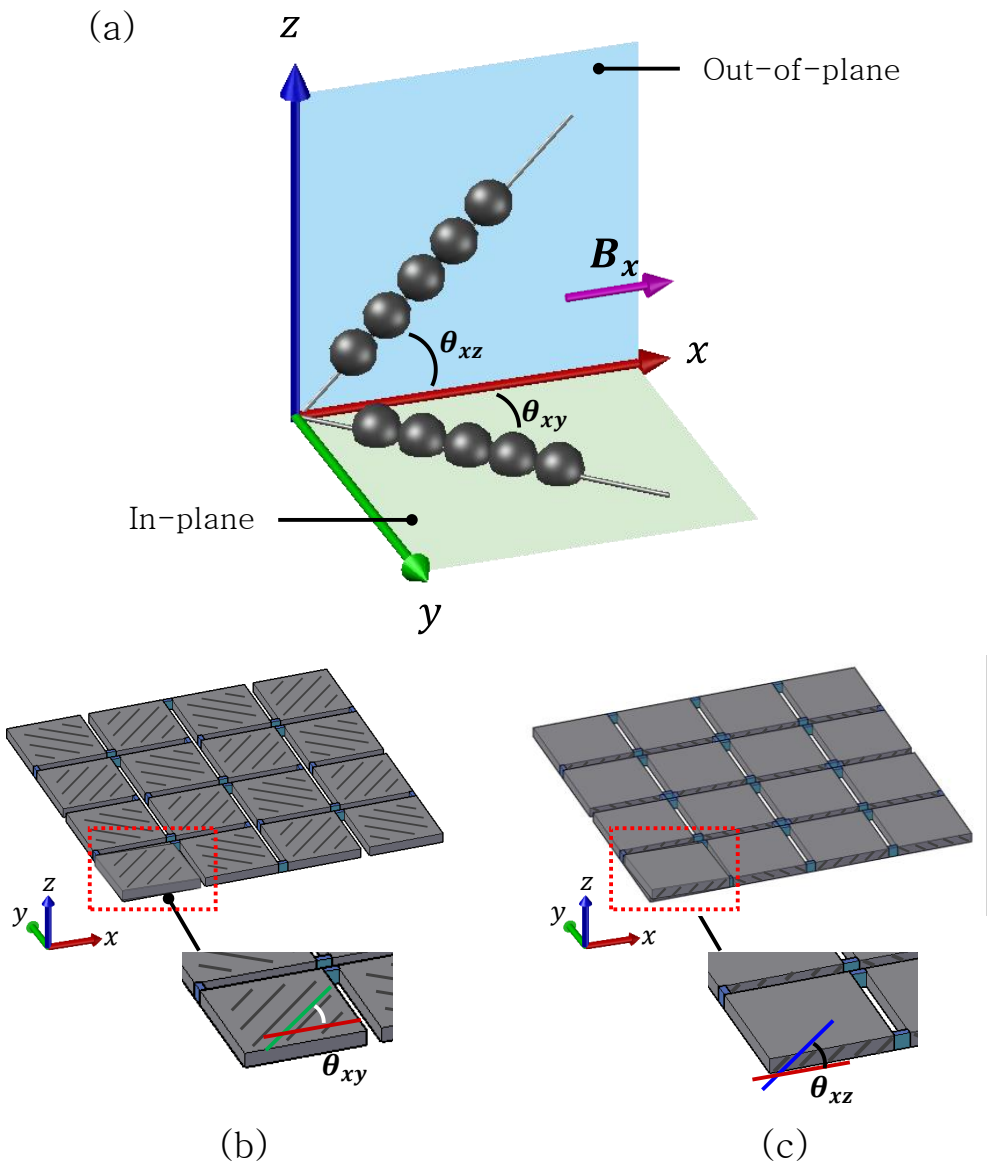

Figure 4. (a) In-plane and out-of-plane MNP chain alignment. The external magnetic field, B_x, is applied along the x-axis. (b) For 2D shape transformation, the MNP chains are aligned in-plane, in the xy-plane, making an angle of θ_{xy} to B_x. (c) For 3D shape transformation, the MNP chains are aligned out-of-plane, in the xz-plane, making an angle of θ_{xz} to B_x.

3.3. Actuation of the Kirigami Patterns

The magnetic actuation of the kirigami patterns arises from the magnetic anisotropic properties of the embedded MNP chains within each square unit, when subjected to an external magnetic field, B_x. As the chains respond to the applied magnetic field to align itself along the direction of the applied field, it causes the square units to rotate. The magnetic actuation of the 2D and 3D kirigami patterns follow the same principle, but differ in terms of the orientation of the MNP chains and the gravity component for the 3D actuation, since the chains are aligned in the xy-plane for 2D patterns, and xz-plane for 3D patterns. It is to be noted that the MNP chains within the 3D kirigami square unit are formed along the thickness.

To get a deeper understanding of the magnetic actuation of the magnetic anisotropic material, the micromechanics of the of material is discussed. In this model, a few assumptions are made: the MNPs are treated as a single-domain, spherical nanoparticles, where the interaction between adjacent chains are neglected, as well as the magnetocrystalline anisotropy and thermal energy. The motion analysis of the kirigami patterns will be performed only on a single square unit for both 2D and 3D actuation, since the square units move independently of each other.

The actuation of kirigami patterns are dependent on the

microscopic magnetic actuation of the MNP chains, and the macroscopic actuation of kirigami shape as a whole. Microscopically, the magnetic actuation deals with the energy of the dipole–dipole interaction, and the applied external magnetic field (Zeeman Energy). These energies in turn generate a magnetic torque, namely the torque on the moments caused by the chaining of the MNPs along the long axis, and the torque on the moments caused by the external magnetic field. On the other hand, the macroscopic actuation deals with the torque caused by the bending of the hinges, and the gravitational torque that acts to cause the 3D actuation. The equilibrium of these torque will bring about the behavior of kirigami actuation.

When the chains within the sample, are placed at an angle θ to the applied magnetic field, B_x, the individual MNP dipoles are rotated by a moment angle, α, as shown in Figure 5. According to [52]-[54], the magnetic dipole–dipole interaction energy E_{12} of one neighboring atom on each side is represented by:

$$E_{12} = \frac{\mu_0}{4\pi}\left(\frac{m_1 m_2}{d^3}\right)\left(\vec{m}_1 \cdot \vec{m}_2 - 3(\vec{m}_1 \cdot \vec{d})(\vec{m}_2 \cdot \vec{d})\right), \quad (1)$$

where $\vec{m}_1$ and $\vec{m}_2$ denote the moments of the MNPs, $\vec{d}$ represents the center–to–center interparticle separation (unit vector), and $\mu_0 = 4\pi \times 10^{-7}\mathrm{kgms^{-2}A^{-2}}$ is the magnetic constant.

For a chain of identical MNPs,

$$\vec{m}_1 = \vec{m}_2 = \vec{m} \ldots \tag{2}$$

$$E_{12} = \frac{\mu_0}{4\pi}\left(\frac{m^2}{d^3}\right)(1 - \cos^2\alpha). \tag{3}$$

For infinitely long chains with 2, 3, 4... neighboring MNPs on each side:

$$E_{1\infty} = 2E_{12}\sum_{1}^{\infty}\frac{1}{n^3}. \tag{4}$$

By referring the Apéry's theorem,

$$\sum_{1}^{\infty}\frac{1}{n^3} = 1.202 \ldots \tag{5}$$

For N MNPs,

$$E = \frac{0.6\mu_0 N}{\pi}\left(\frac{m^2}{d^3}\right)(1 - 3\cos^2\alpha). \tag{6}$$

The magnetic torque, T_m, acting on the moments is therefore:

$$T_m = -\frac{dE_m}{d\alpha}$$

$$= -\frac{1.8\mu_0 N}{\pi}\left(\frac{m^2}{d^3}\right)(\sin 2\alpha). \tag{7}$$

Equivalently, T_c acts opposite to T_m to rotate the sample counterclockwise towards B_x,

$$T_c = \frac{1.8\mu_0 N}{\pi}\left(\frac{m^2}{d^3}\right)(\sin 2\alpha). \tag{8}$$

The Zeeman energy is defined as

$$E_z = -\vec{m}\cdot\vec{B} \tag{9}$$

For N MNPs,

$$E_z = -N\vec{m} \cdot \vec{B}$$
$$= -N\vec{m} \cdot \mu_0 \vec{H}$$
$$= -Nm\mu_0 H \cos(\theta - \alpha). \quad (10)$$

Therefore, the magnetic torque, T_z, acting on the moments due to the external magnetic field, to rotate it counterclockwise towards B_x is:

$$T_z = -\frac{dE_z}{d\alpha}$$
$$= Nm\mu_0 H \sin(\theta - \alpha) \quad (11)$$

The equilibrium of the magnetic moments is,

$$T_z + T_m = 0 \quad (12)$$

$$Nm\mu_0 H \sin(\theta - \alpha) - \frac{1.8\mu_0 N}{\pi}\left(\frac{m^2}{d^3}\right)(\sin 2\alpha) = 0$$

$$H = \frac{1.8m}{\pi d^3}\frac{\sin 2\alpha}{\sin(\theta - \alpha)}. \quad (13)$$

The derived equations above assume that the MNPs assemble into single chains of one MNP wide, along the long axis. However, in reality, the chains are assembled in long straight clusters of multiple MNPs wide. This affects the dipolar interaction of the MNPs along the short axis, and therefore the effective moment must be considered:

$$m' = \gamma m = \gamma M_s V \quad (14)$$

where γ is the disorder parameter, calculated by dividing the remnant moment by the saturation moment, M_s is the saturation magnetization, and $V = \pi d^3/6$ is the volume of the MNP. Since the total volume of

MNP core material is:

$$NV = \frac{fw}{\rho}, \tag{15}$$

where w is the weight of the sample, f is weight fraction of the MNPs, and ρ is the density of the MNPs, the equilibrium can be rewritten as:

$$H = 0.3\gamma M_s \frac{\sin 2\alpha}{\sin(\theta - \alpha)}. \tag{16}$$

Similar to the previous work in [55], the torque in the macroscopic scale involves the bending torque, T_s, at the hinges, as the square units rotate:

$$T_s = -E_s \frac{ab^3}{12l}(\beta - \theta) \tag{17}$$

where E_s is the elastic modulus of the elastomer, β [radians] is the maximum angle that the chain makes with the applied magnetic field B_x, and a, b, l are the thickness, width and length of the hinge, respectively.

By considering a square unit with two hinges, the mechanical equilibrium for a 2D kirigami pattern is:

$$T_s + T_s + T_c = 0 \tag{18}$$

$$-2E_s \frac{ab^3}{12l}(\beta - \theta) + \frac{1.8\mu_0 N}{\pi}\left(\frac{m^2}{d^3}\right)(\sin 2\alpha) = 0$$

Thus,

$$\sin 2\alpha = \frac{ab^3 \rho E_s}{1.8\mu_0 f w \gamma^2 M_s^2 l}(\beta - \theta) \tag{19}$$

On the other hand, to bring about 3D actuation, the gravitational torque, T_g, is considered, in addition to the torque due to the bending of the hinges. Hence,

$$T_g = -\frac{gwL}{2}\sin(\beta - \theta) \tag{20}$$

where g is the gravity, and L is the length of the sample. The mechanical equilibrium relationship for a square unit with two hinges is

$$T_g + T_s + T_s + T_c = 0 \tag{21}$$

$$-\frac{gwL}{2}\sin(\beta - \theta) - 2E_s\frac{ab^3}{12l}(\beta - \theta) + \frac{1.8\mu_0 N}{\pi}\left(\frac{m^2}{d^3}\right)(\sin 2\alpha) = 0$$

Thus,

$$\sin 2\alpha = \left(\frac{ab^3\rho E_s}{1.8\mu_0 f w\gamma^2 M_s^2 l} + \frac{gL\rho}{0.6\mu_0 f\gamma^2 M_s^2}\right)(\beta - \theta) \tag{22}$$

Based on the above equations, through the microscopic and the macroscopic analysis of the torque and its equilibrium, the mathematical model of the 2D and 3D actuation can be achieved. Figure 6 illustrates the theoretical curve of the 2D and 3D actuation of square units consisting of two hinges.

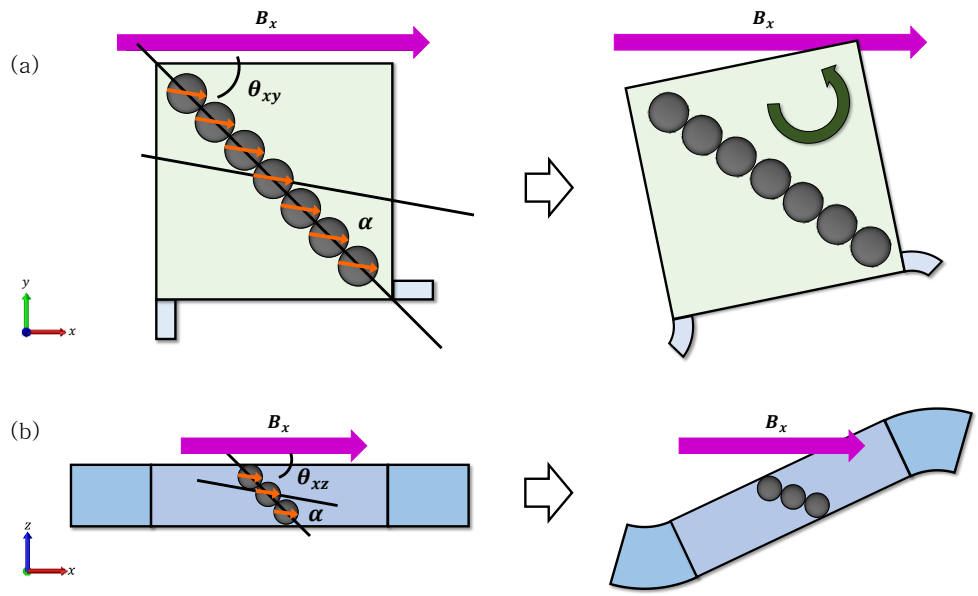

Figure 5. Model of the (a) 2D and (b) 3D kirigami pattern square units when subjected to a uniform magnetic field. B_x. θ_{xy} and θ_{xz} indicate the angle between the MNP chains and B_x, and α depict the angle between the moment and the chains.

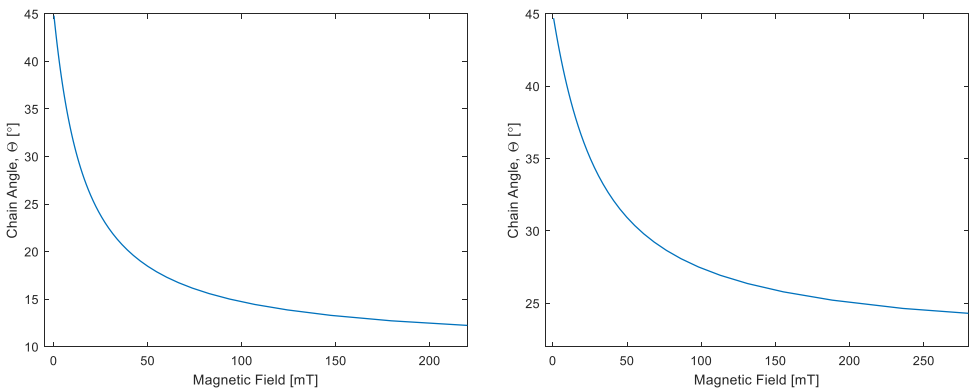

(a) (b)

Figure 6. Theoretical curves of the (a) 2D and (b) 3D kirigami square units.

Chapter 4. Design and Fabrication

This chapter describes the design and the fabrication method of the magnetic kirigami patterns. Schematic illustrations of the chain directions and the corresponding actuated profiles are shown. A detailed fabrication method, including the dimensions and the materials used, can be found in this chapter.

4.1. Design of the Kirigami Patterns

In this study, the designs of the kirigami patterns consists of sixteen square units that are joined together by hinges. The designs of the 2D and 3D kirigami patterns are similar to each other, with differences at the 'cuts' on the pattern, i.e. the placement of the hinges, and the direction of the MNP chains within each square unit.

4.1.1. 2D Kirigami Patterns

Two 2D kirigami patterns are introduced in this study: the rotating square pattern [8], [56], [57] and the fractal cut pattern [16], [20], [21]. As emphasized in Section 3.2, MNP chains within the 2D pattern are aligned in-plane along the xy-plane, at an angle of θ_{xy} with respect to the applied magnetic field, B_x. In the rotating square unit

pattern, the MNP chains within each square units are aligned at $\theta_{xy} = \pm 45$°, where they are joined together alternatively by hinges, as shown in Figure 7 (a). Likewise, the chains of the fractal cut patterns are aligned at $\theta_{xy} = \pm 26.5°$ and $\theta_{xy} = \pm 63.5°$, as depicted in Figure 7. In addition, as illustrated in Figure 7, the schematic of the actuated 2D shape is shown alongside the original 2D kirigami pattern, where the chains within each square units align with the applied external magnetic field.

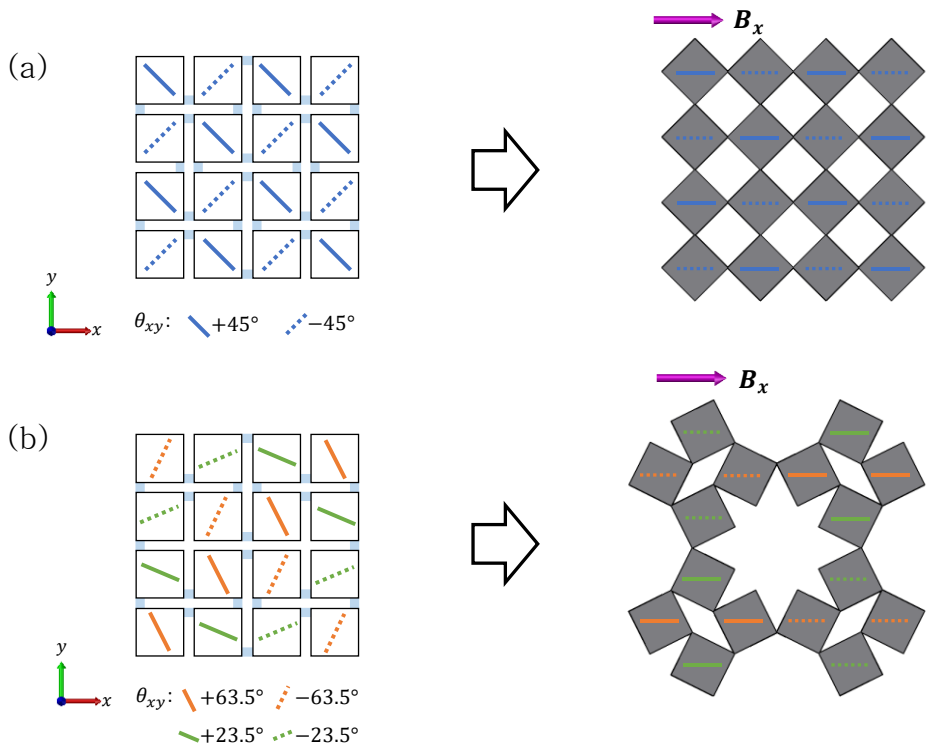

Figure 7. Schematic of the 2D kirigami pattern designs and its actuated profile. (a) the rotating square pattern, and (b) the fractal cut pattern. The hinges in the actuated schematic are omitted for simplicity. Pink arrows indicate the direction of the magnetic field B_x.

4.1.2. 3D Kirigami Patterns

Three 3D kirigami patterns are used in this study to demonstrate the 3D shape morphologies. The 3D kirigami patterns consists of alternating squares that are aligned out-of-plane at an angle of $\theta_{xz} = \pm 45°$, along the xz-plane, with respect to the direction of B_x. Similar to the 2D kirigami patterns, the square units are joined together alternatively by hinges. Each 3D kirigami design consists of the same square unit pattern, and differ only by the placement of the hinges, where the void areas simulate the horizontal and vertical cuts. The proposed 3D patterns are termed A, B, and C, and their shape morphologies are depicted in Figure 8.

4.2. Fabrication Method

The fabrication method of the kirigami patterns involves a two-step process. The first step entails the functionalization of the composite by aligning the MNPs into chains. The second step involves the assembly of the square units by connecting them together with hinges.

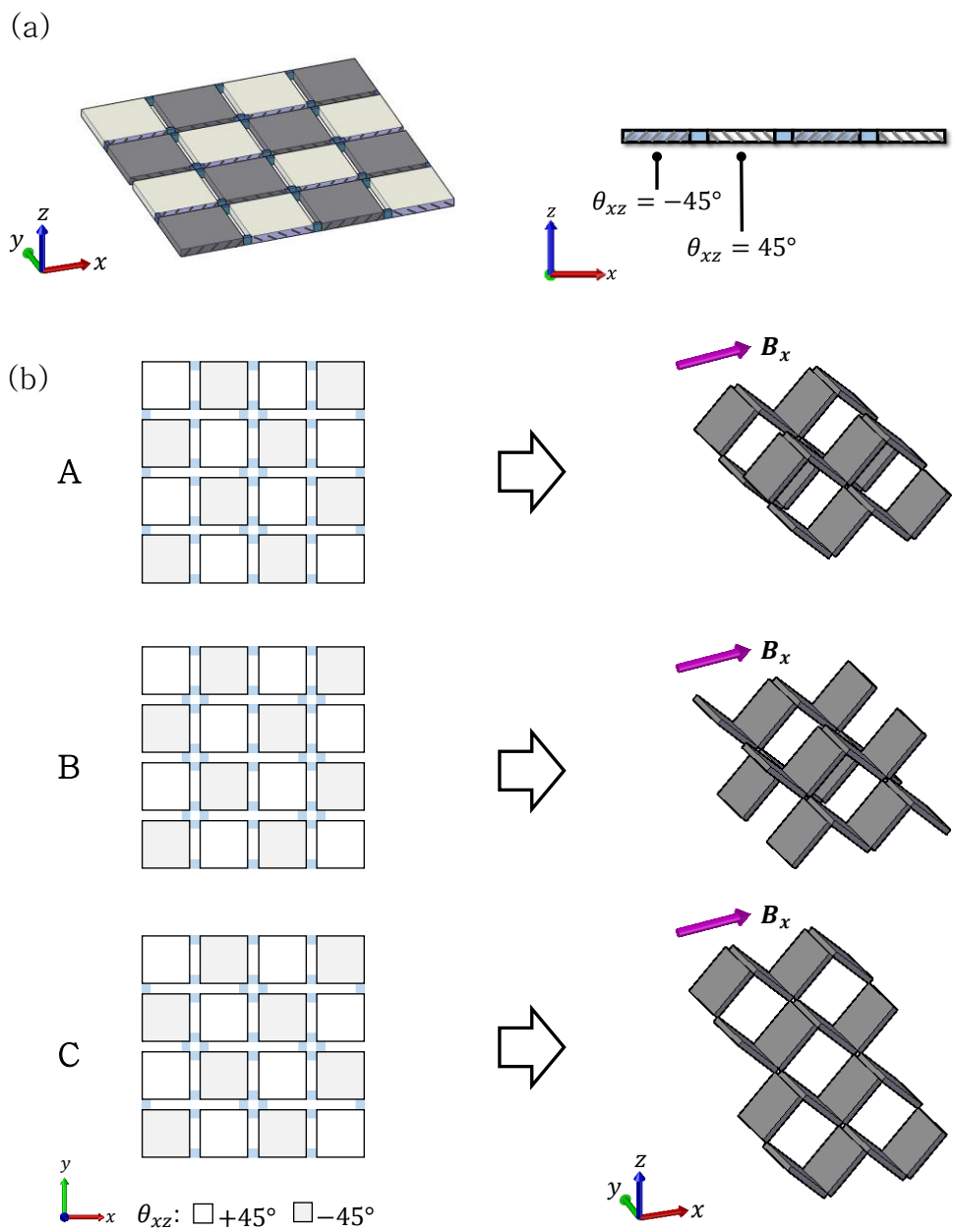

Figure 8. Schematic of the 3D kirigami pattern designs and its actuated profile. (a) arrangement of the square units, and (b) hinge pattern of shapes A, B, and C, and its actuated profile. The hinges in the actuated schematic are omitted for simplicity. Pink arrows indicate the direction of the magnetic field B_x.

4.2.1. Mold

Two types of molds are used in fabricating the kirigami pattern: the alignment mold and the assembly mold, where they are used in the first and second step of the fabrication process, respectively. Both molds are fabricated using patterned vinyl adhesive that is placed on top of a clear acrylic sheet (1.3 mm thick). The patterns are first designed on a 3D CAD software (AutoCAD, Autodesk) and transferred to Silhouette Studio, to be cut by the Silhouette CAMEO 2 vinyl cutter. Fabricating molds using a vinyl cutter is faster, cheaper, and offers thinner profiles (approximately 200 μm) than that produced by 3D printing.

The alignment mold and the assembly mold are shown in Figure 9. The alignment mold consists of several square units, while the assembly mold consists of the complete kirigami pattern: the square units and the connecting hinges. The dimension of the square units used in this study and the variation of the hinge size are summarized in Table 1. c indicate the length of the square units, b and l depict the width and the length of the hinges, respectively. For all shapes, the width of the hinge is kept at 0.4 mm.

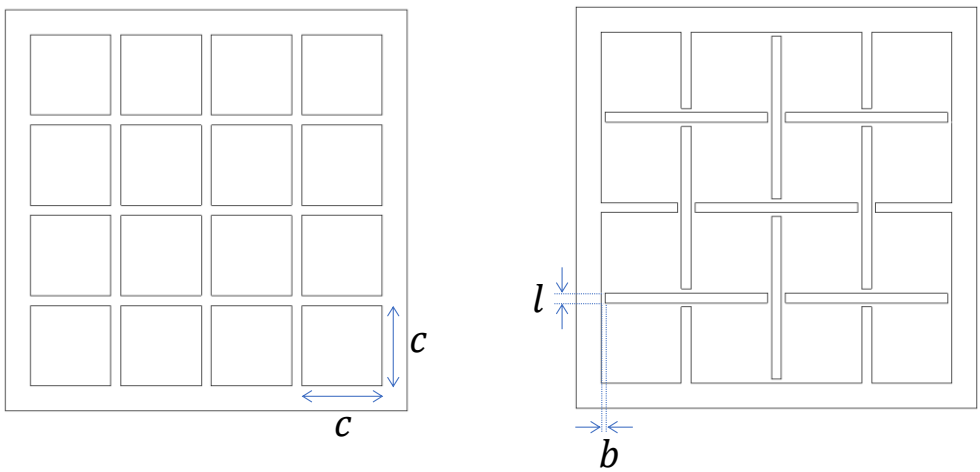

(a) (b)

Figure 9. Schematic illustration of the (a) alignment mold and the (b) assembly mold. c indicate the length of the square units, b and l depict the width and the length of the hinges, respectively.

Table 1. Dimensions of the square units and the hinges of the kirigami patterns.

Shape		c [mm]	l [mm]
Rotating square	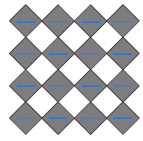	8	1
Fractal cut	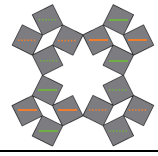		
A	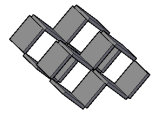	6	1, 2
		8	1, 2
B	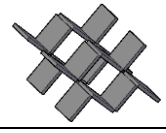	8	1
C	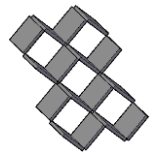		

4.2.2. Material Preparation

Prior to aligning the MNP chains, the magnetic-elastomer composite must be prepared. First, the two parts, Part A and Part B, of the Xinuslab (SH2115) silicone elastomer are mixed in a 1:1 ratio. Once they are well incorporated, 20 wt% of Fe_3O_4 iron oxide nanoparticles (Sigma-Aldrich, 637106) with an average size of 50 nm are added to the silicone elastomer mixture and mixed. The magnetic-elastomer composite is then immediately poured into the assembly mold, and placed in the uniform magnetic field, to be functionalized.

4.2.3. Functionalization of the Square Units

The direction of which the MNP chains are to be aligned is simply determined by the morphology of the actuated shape with respect to the direction of the magnetic field, B_x, which is the direction of the external uniform magnetic field used to align and actuate the kirigami patterns. The alignment is performed by placing the alignment mold consisting of the shape of the square units and the uncured magnetic-elastomer composite in a uniform magnetic field of 30 mT that is generated from the electromagnet. An acrylic sheet is placed on top of the mold to keep the material inside the mold. While the composite is uncured, the MNPs move and self-assemble into chains in the direction of the applied magnetic field, such that when the elastomer

matrix is cured, the chains are permanently embedded within the matrix. The curing time of the composite is approximately 30 minutes.

In-plane and out-of-plane alignment of the MNP chains are performed by placing the mold at an angle to B_x, in the corresponding plane, as shown in Figure 10. To align the MNP chains in-plane, the mold is placed along the xy-plane, at an angle of θ_{xy} with respect to B_x (see Figure 10 (a)). On the other hand, to align the chains out-of-plane, the mold must be elevated in the z-axis, at an angle of θ_{xz} to B_x. Due to this reason, a jig is used to lift up the mold, as shown in Figure 10 (b). The jig is fabricated using a 3D printer (Sindoh, 3DWOX), where it is designed in a 3D CAD software (AutoCAD, Autodesk).

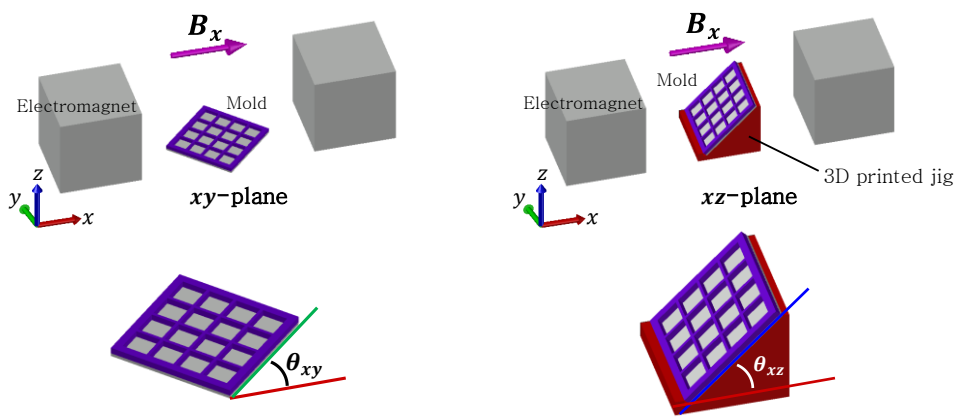

(a) (b)

Figure 10. Chain alignment method for (a) 2D and (b) 3D kirigami patterns. Pink arrows indicate the direction of the magnetic field B_x.

4.2.4. Assembly of the Square Units

The second step of the fabrication process involves the assembly of the aligned kirigami square units. The square units are removed from the alignment mold, and trimmed with a craft knife to remove the excess. Each square units are placed inside a second mold, the assembly mold, consisting of the kirigami pattern and its hinges. The assembly is done by means of the silicone elastomer. The material is prepared by missing Part A and Part B in a ratio of 1:1 and degassed in a desiccator to remove the air bubbles. The elastomer is then added to the hinge areas of the mold. To ensure uniform thickness of the hinges and the square units, the mold is covered using a thin acrylic sheet. Once the elastomer is cured, the kirigami pattern is removed from the mold and trimmed to remove excess elastomer.

Chapter 5. Experiment

This chapter offers detailed explanation of the experimental design, conditions, setup, and procedure. Five experiments are conducted in this study to evaluate the 2D and 3D actuation of the kirigami patterns.

5.1. Experimental Design

The experiments of the 2D and 3D kirigami pattern aims to analyze the shape transformation capabilities when subjected to a uniform external magnetic field that is provided by an electromagnet. The experiment common to both patterns evaluates the angle that the square units make with respect to the applied magnetic field, B_x. For 2D kirigami patterns, the experiment is performed on the surface of water, in order to provide a frictionless actuating space. On the other hand, the experiment of the 3D kirigami patterns are performed on the surface of the workspace. In addition, for 3D kirigami patterns, the 3D shape transformation capabilities are further analyzed by actuating the pattern in three different conditions: underwater, suspended, and on the surface of an object. To analyze strength of the 3D kirgami patterns, weights of 0.03 g and size 5 x 10 mm are made using paper,

and are placed on top of the structure. Lastly, to observe the behavior of the 3D kirigami patterns, the direction of the magnetic field is changed from the horizontal field, B_x, to the vertical field, B_z. All data are collected using a camera. The experiments conducted in this study are summarized below:

1. 2D actuation of kirigami pattern
2. 3D actuation of kirigami pattern
3. 3D morphologies of kirigami patterns in different conditions (underwater, suspended, and on top of objects)
4. 3D morphologies with weights
5. Behavior of 3D kirigami patterns under vertical magnetic field, B_z.

5.2. Experimental Conditions

The experiments in this study are performed under a uniform magnetic field, B_x, in the horizontal (x) direction, that is generated by an electromagnet. The electromagnet poles are placed 11.5 cm apart, providing a workspace of 11.5 x 12 cm. To operate the electromagnet, the voltage is set at 60 V, with a current range of 0-15 A. The magnetic field is varied by changing the supply current of the electromagnet, resulting in a magnetic field range of 0-270 mT. For experiments that involve the analysis of the angle, the current is varied

in increments of 0.5 A.

In most experiments, anchors are needed to prevent the kirigami patterns from getting attracted to the electromagnet. For 2D kirigami patterns, graphite rods are used to anchor the shape by placing the rods underneath the kirigami pattern, slightly touching one of the square units. On the other hand, for 3D kirigami patterns, graphite rods are pinned perpendicularly in the middle of the kirigami shape.

In the final experiment (5) of the 3D kirigami pattern, the vertical magnetic field in the z-direction is generated by the top surface of one of the poles of the electromagnet. The magnetic field generated is roughly uniform, and can be used to demonstrate the 3D shape transformation.

5.2. Experimental Setup

The experimental setup of the 2D and 3D actuation is displayed in Figure 11. It consists mainly of an electromagnet and a camera. The morphologies of the kirigami patterns are performed in the workspace in between the poles of the electromagnet. Grid paper with 5 mm square grids and a ruler are placed for size comparison. A water basin is placed in between the electromagnetic poles for experiments that require water.

The experimental setup of the last experiment (5), is similar to

that used in experiment 1-4. However, since the vertical magnetic field is required in this experiment, the 3D kirigami pattern is place on top of the pole of the electromagnet, for the vertical magnetic field, B_z.

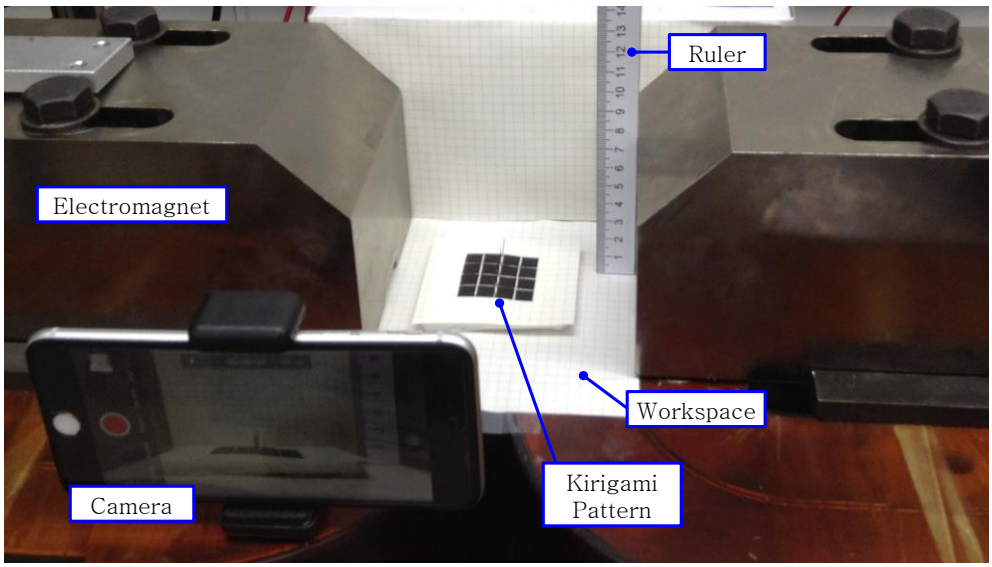

Figure 11. Experimental Setup.

5.3. Experimental Procedure

Experiments 1 and 2 follow the same procedure. The 2D and 3D kirigami patterns are actuated under a uniform magnetic field of 0-270 mT, with increments of roughly 10 mT. These increments are performed by adjusting the current of the electromagnet at increments of 0.5 A, in the range of 0-14 A. The differences of the two experiments is the actuating platform. The experiment of the 2D

kirigami patterns are performed on the surface of water, while the 3D kirigami patterns are performed on the surface of the workspace.

In experiment 3, the 3D kirigami patterns are actuated in different conditions: underwater, suspended, and on top of objects. Underwater actuation is performed by suspending the patterns in a water basin. To suspend the patterns, the 3D kirigami patterns are placed on top of a graphite rod. Lastly, the actuation on the surface of objects are performed by placing the 3D kirigami patterns on top of objects of different shapes: 3 cm sphere, 4 cm sphere, and arbitrary shape. The magnetic field used in this experiment is 270 mT.

The experimental procedure of experiment 4 is performed by applying a constant magnetic field of 270 mT to the 3D actuators placed on the surface of the workspace. Rectangular paper of different weights are stacked on top of the structure to determine how much the 3D kirigami pattern can hold up to the applied mass.

Lastly, experiment 5 is performed on top of one of the electromagnet poles, to obtain the vertical magnetic field, B_z. The actuation is performed over a range of magnetic field of 0–125 mT, where the current is varied at 0.5 A increments within the current range of 0–14 A.

Chapter 6. Results

Chapter 6 provides the results of the all the five experiments conducted in this study. The obtained results are compared with the proposed mathematical model. In addition, the magnetic properties are measured using the vibrating sample magnetometer (VSM) and characterized with an optical microscope.

6.1. 2D Actuation of Magnetic Kirigami Patterns

When the 2D kirigami patterns are subjected to a uniform magnetic field, each square unit simultaneously rotate in order to align the embedded chains parallel to the direction of the applied magnetic field. The 2D actuated morphologies of the 2D kirigami patterns are illustrated in Figure 12. The results show that the 2D shape morphology of the fractal cut pattern match well with the schematic diagram. However, there are slight differences to the rotating square pattern, which might be due to the size of the hinges that are preventing the pattern from achieving the desired shape morphology. This causes an increase in the area of the kirigami pattern. Since the square units are aligned in-plane along the xy-plane, the resulting actuated shape is also in the same plane.

The relationship between the chain angle that the 2D kirigami pattern makes with the applied magnetic field is shown in Figure 13, where the experimental data is plotted against the theoretical curve. The results show a decrease in the chain angle as the magnetic field increases, indicating that the square units move to align the chains with the magnetic field.

6.2. 3D Actuation of Magnetic Kirigami Patterns

When the 3D kirigami patterns are subjected to a uniform magnetic field, each square unit buckle up along the z-axis simultaneously in order to align the embedded chains with the direction of the magnetic field. The 3D actuated morphologies of the 3D kirigami patterns are shown in Figure 14. Experimental results show that the kirigami pattern can buckle up in 3D. However, the maximum angle that the chains can make is 28°, as shown in Figure 15. This could be due to the fact that the 3D kirigami pattern do not have enough energy to actuate against gravity that is pushing down on the pattern. This might also be the main reason why the experimental data do not match well with the theoretical prediction.

3D actuation can be performed in many conditions, as shown in Figure 16. On the surface of water, the 3D kirigami patterns can only be actuated slightly since the surface tension of water surface is

preventing the movement of the along the z-axis. Hence, shapes A, B, and C, are submerged underwater. When in water, the kirigami actuators float by maintaining the actuated shape. Due to the spontaneous response of the 3D kirigami pattern, it can be confirmed that by varying the ‘cuts’ (or the placement of the hinges) on the pattern, several 3D actuation morphologies can be performed. In dry conditions, the kirigami actuators can either be actuated on a flat surface, suspended in midair, or even on surfaces of different shapes.

To analyze the strength of the 3D kirgami pattern, paper weights are placed on top of 8 mm and 6 mm kirigami patterns, as shown in Figure 17. By stacking paper weights on top of each other until the weight reaches the actuated surface, the amount of weight that the kirigami patterns can hold can be determined. 8 mm kirigami patterns are able to hold larger weights than the 6 mm patterns. 8 mm actuators can hold weights up to 0.2 g, and 0.1 g for 6 mm. This confirms that the larger the size, the more weight it can hold.

Lastly, the behavior of 3D kirigami patterns under a vertical magnetic field, B_z, are observed. As shown in Figure 18, the 3D morphologies of shapes A and B match very well with the schematic illustration, where the square units are able to make an angle close to the theoretical value of 45°. In addition, Figure 19 confirms that by using the vertical magnetic field, better 3D actuation can be achieved.

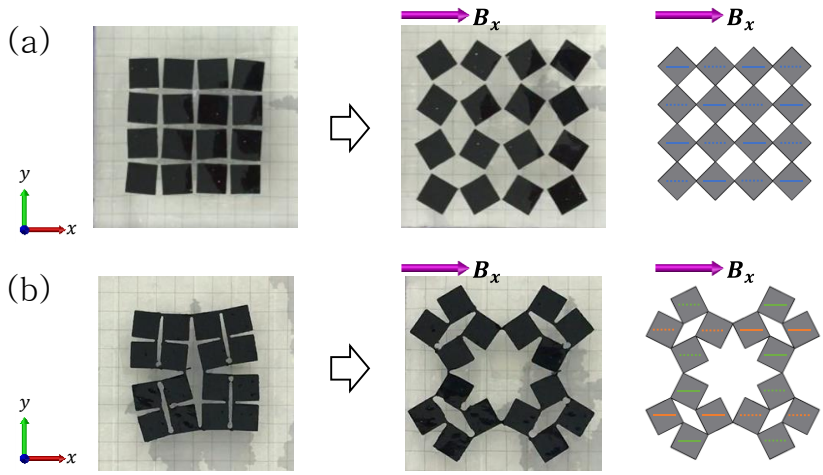

Figure 12. Actuation of the 2D kirigami patterns and its schematic illustrations: (a) rotating square pattern and (b) fractal cut pattern (from previous study [55]). The hinges in the actuated profiles are omitted for simplicity. Pink arrows indicate the direction of the magnetic field B_x.

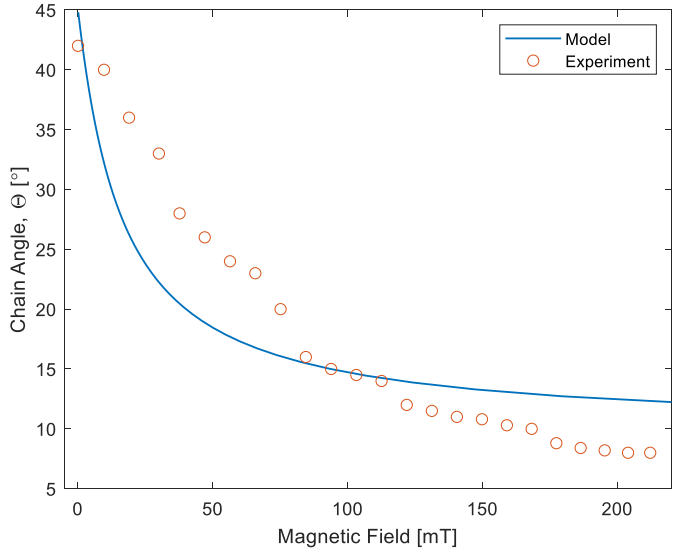

Figure 13. Comparison of the experimental data with the theoretical values of the 2D kirigami pattern to see the relationship between the chain angle and the applied magnetic field.

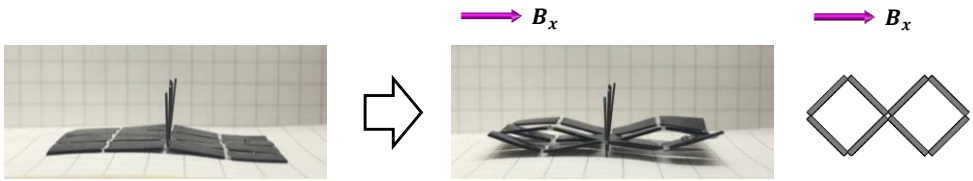

Figure 14. Actuation of the 3D kirigami patterns at 270 mT and its front view schematic illustrations of shape A. The hinges in the schematic are omitted for simplicity. Pink arrows indicate the direction of the magnetic field B_x.

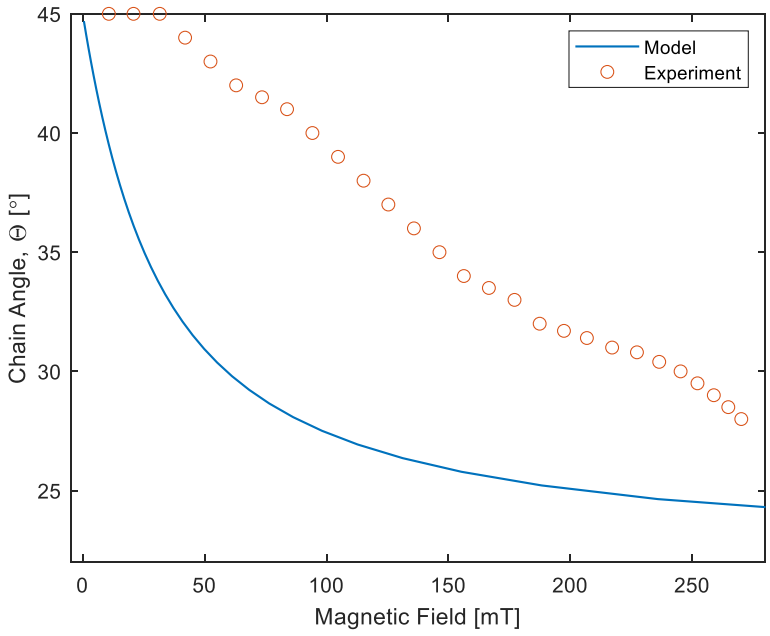

Figure 15. Comparison of the experimental data with the theoretical values of the 3D kirigami pattern to see the relationship between the chain angle and the applied magnetic field.

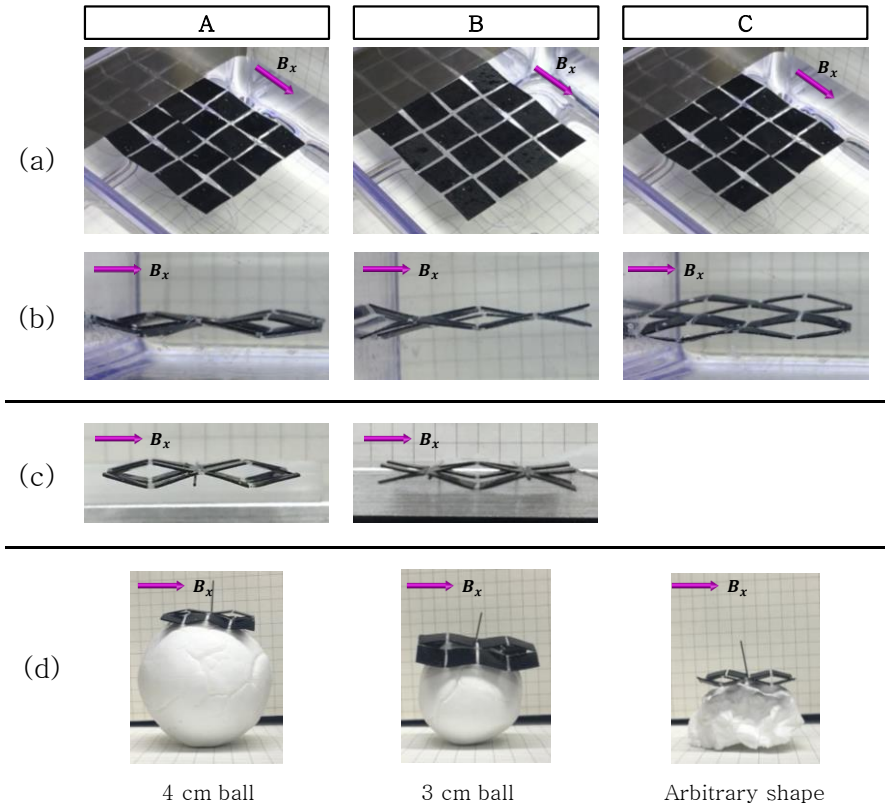

Figure 16. 3D morphologies of 3D kirigami patterns in different conditions: (a) on surface of water, (b) underwater, (c) suspended in midair and (d) on top of objects. Pink arrows indicate the direction of the magnetic field B_x, where $B_x = 270\ \mathrm{mT}$.

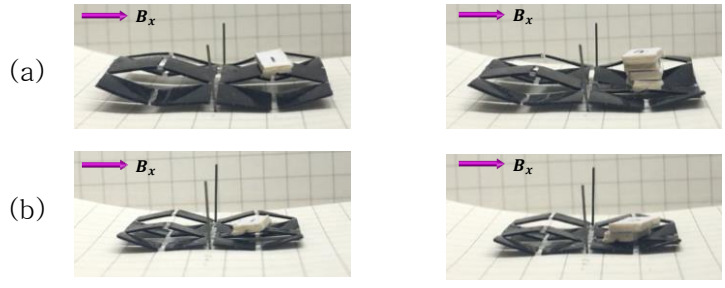

Figure 17. 3D actuation of (a) 8 mm and (b) 6 mm kirigami pattern when weight is put on top of the actuated pattern. Pink arrows indicate the direction of the magnetic field B_x, where $B_x = 270\ \mathrm{mT}$.

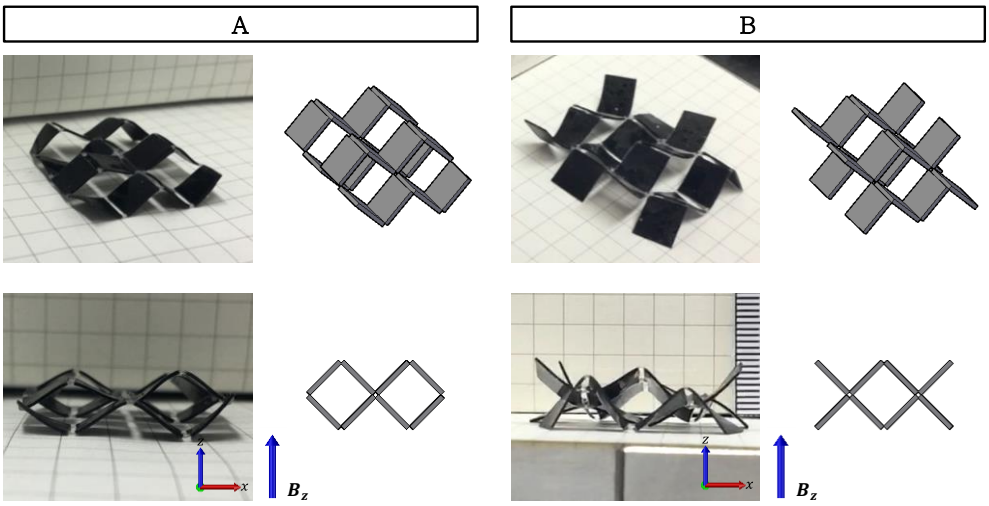

Figure 18. Behavior of 3D kirigami patterns under vertical magnetic field, B_z. Blue arrows indicate the direction of the vertical magnetic field B_z, where $B_z = 128\,\mathrm{mT}$.

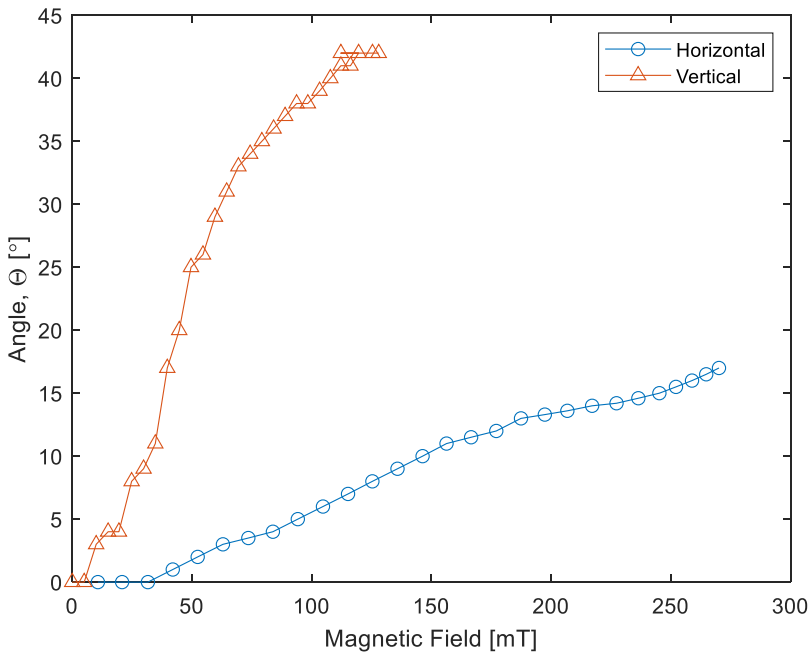

Figure 19. Comparison of the angles that the 3D kirigami pattern make when subjected to a horizontal, B_x, and vertical, B_z, magnetic field. The angles are measured in the xz-plane, with respect to the x-axis.

6.3. Magnetic Properties and Characterization

To confirm that the kirigami patterns have magnetic anisotropy square unit samples of parallel, perpendicular, 45 degree in-plane, 45 degree out-of-plane, and unaligned MNP chains are prepared. These samples are analyzed by the vibrating sample magnetometer (VSM) and characterized with an optical microscope.

6.3.1. Vibrating-sample magnetometer

The magnetic properties of the kirigami patterns are characterized by means of a vibrating-sample magnetometer (Lake shore, VSM-7410). Square unit samples of 8x8 mm were prepared by aligning the MNP chains in-plane and out-of-plane at different angles. For in-plane samples, the chains are aligned parallel, perpendicular, and 45-degree to the direction applied magnetic field. Similarly, for out-of-plane samples, the chains are aligned at 45-degree out-of-plane. In addition, an unaligned sample is also prepared. Hysteresis curves of each samples are obtained by using a magnetic field ranging from -300 to 300 mT, and are compared in Figure 20 and Figure 21.

As illustrated in Figure 20, the in-plane samples show that chains that are parallel to the direction of the magnetic field have the highest magnetization, since the embedded MNP chains are aligned with the

direction of the magnetic field. At this position, the chains have the lowest energy and therefore is the most energetically favorable. Perpendicular chains on the other hand, have the lowest magnetization, since the chains are aligned 90° to the field. Therefore, the 45-degree chains have higher magnetization than the perpendicular samples, but less than that aligned parallel. From the hysteresis loops, it is confirmed that samples with direction, i.e. magnetic anisotropy, have higher magnetization than those that are not aligned, since the parallel, perpendicular, and 45-degree all have higher magnetization curves than the unaligned sample. Furthermore, this also indicate that MNP chains causes that samples to be directional dependent, and hence allowing anisotropic actuation of the kirigami patterns.

Figure 21 show the hysteresis loops of samples that are parallel (in-plane) and 45 degrees out-of-plane. In-plane samples have higher magnetization than out-of-plane samples since it has longer chains across the surface. Out-of-plane samples on the other hand have shorter chains, as they are aligned along the thickness of the sample.

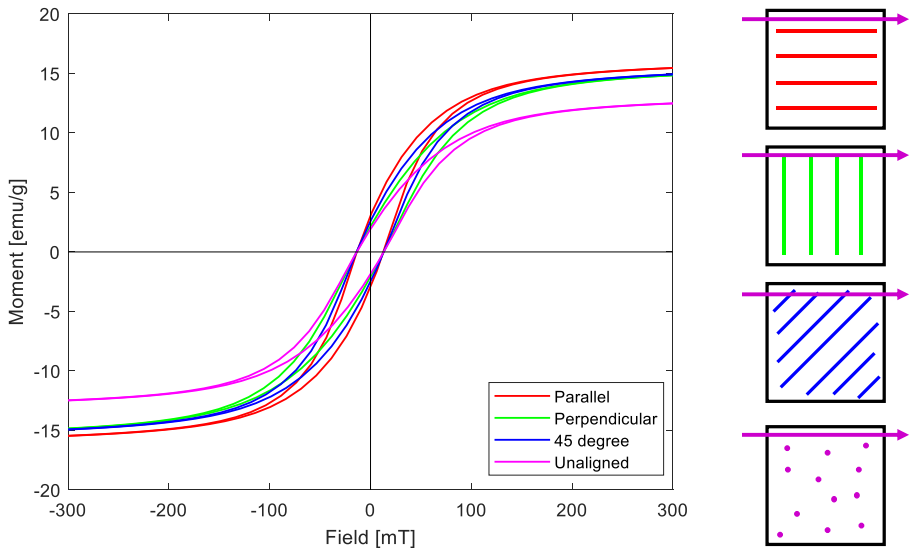

Figure 20. Comparison of the hysteresis curves of the square units that are aligned in-plane parallel, perpendicular and 45-degrees to the magnetic field B_x, and unaligned. Pink arrows indicate the direction of the magnetic field B_x.

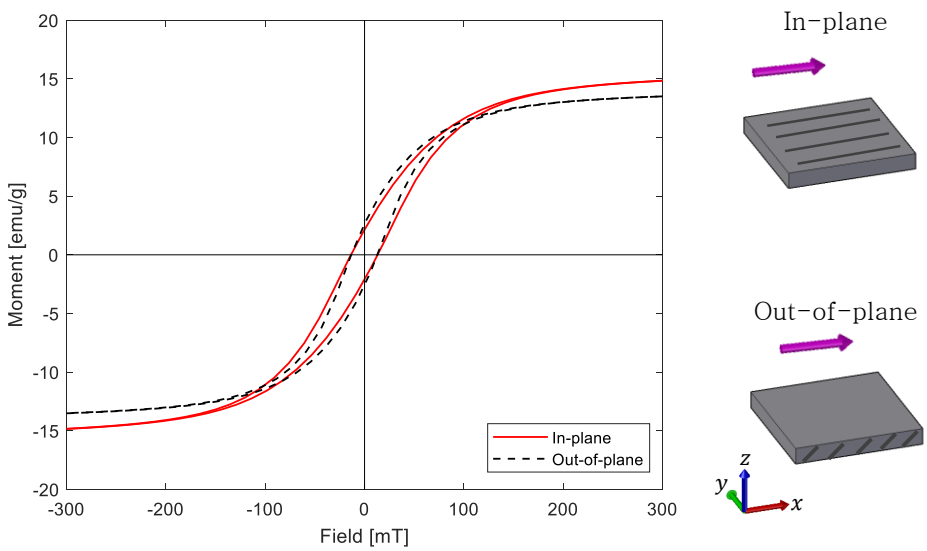

Figure 21. Comparison of the hysteresis curves of the square units that are aligned in-plane and out-of-plane (at 45 degrees). Pink arrows indicate the direction of the magnetic field B_x.

6.3.2. Optical Microscope

Optical microscopic images of square unit samples are taken to show the morphologies of the MNPs. Figure 22 (a) depict the MNPs of an unaligned sample, where no chains are formed. This is due to the fact that the material is not functionalized, and the MNPs are randomly distributed throughout the composite. On the other hand, Figure 22 (b) show even chain distribution at 45°, since the MNPs are aligned at 45° in-plane, along the xy-plane. However, when the MNPs are aligned out-of-plane in the xz-plane, the chain morphologies are shown in Figure 22 (c). Although the image looks 3D, it is not confirmed that the sample has magnetic anisotropic properties. Therefore, the cross-section image along the xy-plane is taken, as shown in Figure 22 (d). Since the dark lines at 45-degree angle of the cross-section indicate the MNP chains, the magnetic anisotropy of the 3D kirigami pattern is confirmed.

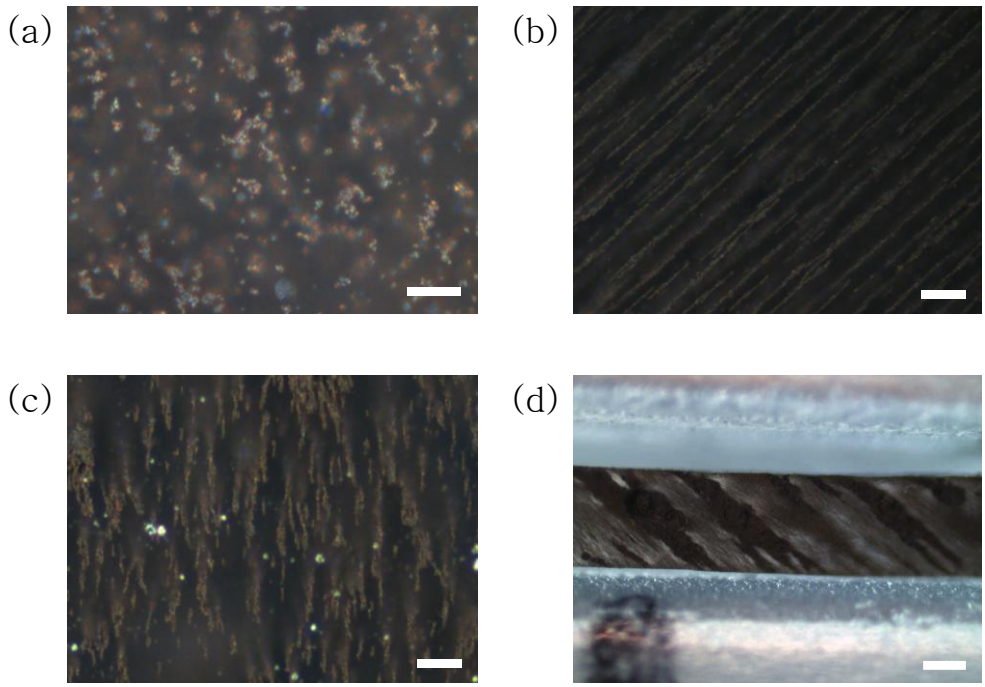

Figure 22. Optical microscopic images of (a) unaligned, (b) 45 degree in-plane, (c) 45 degree out-of-plane, and (d) cross-section of (c) square unit samples. Scale bars of (a), (b), and (c) are 25 μm and 200 μm for (d).

Chapter 7. Discussion

This study has demonstrated the remote 2D and 3D actuation of magnetic kirigami patterns by programming the magnetic anisotropy of each square units and assembling each part separately. This therefore allow the kirigami patterns to be controllable under an applied uniform magnetic field. The 2D and 3D actuation mechanism of the kirigami patterns follow the same concept where due magnetic anisotropy, the hinges rotate as the embedded chains within the square units turn to align with the direction of the applied external magnetic field. Depending on the direction and the angle that the chains make with respect to the applied field as well as the cut designs of the kirigami patterns, a variety of kirigami structures can be fabricated. In addition, this study has demonstrated the actuation of kirigami patterns in both wet and dry conditions, such as underwater, on flat and curved surfaces. The fabrication method used in this study is simple and can be reproduced by those with access of an electromagnet, since the materials used are widely accessible. This not the case for other studies since the physical apparatus are not commercially available and need to be custom made. Hence, this study can provide a hands-on experience for students on the application of magnetic anisotropy

and to get an understanding of its principles. Furthermore, the remote actuation of other kirigami patterns or auxetic structures can also be studied. For instance, instead of using square units can be replaced by other shapes such as triangles, pentagons, etc. This research therefore provides the preliminary research for futures studies and applications.

However, the limitations of this study lie on the fact that the kirigami patterns cannot achieve the theoretical morphologies when using the horizontal magnetic field as the actuating field. Due to this reason, there are large deviations between the experimental data and the model. In addition, to prevent the kirigami patterns from being attracted to the electromagnet, anchors are required. Although remote actuation can be achieved, the kirigami patterns are not able to freely move around within the workspace. Moreover, the size of the kirigami patterns are still too big to be used in very small spaces such as inside the human body. Therefore, further studies on the size reduction of the kirigami patterns can be performed. However, one of the concerns on the size reduction of kirigami patterns is that the hinges must be very small, as they are also responsible for the 2D and 3D actuation, as well as to bring the kirigami patterns back to its original shape. The elimination of these hinges can also be studied, where the deformation of at the connecting areas of the square units must be considered.

Chapter 8. Conclusion

Remote actuation of kirigami patterns in 2D and 3D can be realized through in-plane and out-of-plane alignment of the MNPs, respectively. It is shown that by making different cut designs, several shape transforamtion can be obtained. With the in-plane alignment of MNPs, 2D actuation can be demonstrated through the rotation of square units and fractal patterns, which resulted in auxetic structures of negative Poisson number. On the other hand, out-of-plane alignment of MNPs could give rise to 3D buckling and elevation of kirigami patterns, where these deformations could also be seen in mechanical metamaterials. The actuation of kirigami patterns can be performed in both wet and dry conditions. In addition, the kirigami patterns in this study can react to both the horizontal and vertical magnetic fields. Untethered actuation of kirigami patterns therefore have potential applications in areas such as drug delivery, medical patches, and artificial valves.

As an extension to this study, the model of the kirigami patterns will be further improved and investigated. In addition, studies on other types of kirigami patterns and unit shapes will be performed to evaluate the feasibility of the magnetic control of kirigami patterns.

References

[1] J. Cui, F. R. Poblete, and Y. Zhu, “Origami/Kirigami-Guided Morphing of Composite Sheets,” *Adv. Funct. Mater.*, vol. 28, no. 44, pp. 1–7, 2018.

[2] B. G. G. Chen *et al.*, “Topological Mechanics of Origami and Kirigami,” *Phys. Rev. Lett.*, vol. 116, no. 13, pp. 1–5, 2016.

[3] R. M. Neville, F. Scarpa, and A. Pirrera, “Shape morphing Kirigami mechanical metamaterials,” *Sci. Rep.*, vol. 6, no. August 2015, pp. 1–12, 2016.

[4] D. M. Sussman *et al.*, “Algorithmic Lattice Kirigami: A Route to Pluripotent Materials,” 2015.

[5] L. Xu, T. C. Shyu, and N. A. Kotov, “Origami and Kirigami Nanocomposites,” *ACS Nano*, vol. 11, no. 8, pp. 7587–7599, 2017.

[6] Y. Tang and J. Yin, “Design of cut unit geometry in hierarchical kirigami-based auxetic metamaterials for high stretchability and compressibility,” *Extrem. Mech. Lett.*, vol. 12, pp. 77–85, 2017.

[7] X. Ren, R. Das, P. Tran, T. D. Ngo, and Y. M. Xie, “Auxetic metamaterials and structures: A review,” *Smart Mater. Struct.*, vol. 27, no. 2, 2018.

[8] R. Gatt *et al.*, “Hierarchical Auxetic Mechanical Metamaterials,”

Sci. Rep., vol. 5, pp. 1–6, 2015.

[9] M. Mir, M. N. Ali, J. Sami, and U. Ansari, "Review of mechanics and applications of auxetic structures," *Adv. Mater. Sci. Eng.*, vol. 2014, no. September, 2014.

[10] R. Critchley, I. Corni, J. A. Wharton, F. C. Walsh, R. J. K. Wood, and K. R. Stokes, "A review of the manufacture, mechanical properties and potential applications of auxetic foams," *Phys. Status Solidi Basic Res.*, vol. 250, no. 10, pp. 1963–1982, 2013.

[11] H. M. A. Kolken and A. A. Zadpoor, "Auxetic mechanical metamaterials," *RSC Adv.*, vol. 7, no. 9, pp. 5111–5129, 2017.

[12] M. A. Fortes and M. T. Nogueira, "The poisson efect in cork," *Mater. Sci. Eng.*, vol. A122, pp. 227–232, 1989.

[13] Lakes Roderic, "Foam Structures with a Negative Poisson ' s Ratio," *Science (80-.).*, vol. 235, pp. 1038–1040, 1987.

[14] E. Science and G. Britain, "chiral honeycombe. Poisson's ratio. 1. INTRODUCTION Cellular solids are used widely in a variety of engineering applications. In particular," *Science (80-.).*, vol. 39, no. 3, 1997.

[15] R. Zhao, S. Lin, H. Yuk, and X. Zhao, "Kirigami enhances film adhesion," *Soft Matter*, vol. 14, no. 13, pp. 2515–2525, 2018.

[16] S. Yang, I.-S. Choi, and R. D. Kamien, "Design of super-conformable, foldable materials via fractal cuts and lattice

kirigami," *MRS Bull.*, vol. 41, no. 2, pp. 130–138, 2016.

[17] R. Ma, C. Wu, Z. L. Wang, and V. V. Tsukruk, "Pop-Up Conducting Large-Area Biographene Kirigami," *ACS Nano*, vol. 12, no. 10, pp. 9714–9720, 2018.

[18] H. Ko and A. Javey, "Smart Actuators and Adhesives for Reconfigurable Matter," *Acc. Chem. Res.*, vol. 50, no. 4, pp. 691–702, 2017.

[19] J. A. Fan *et al.*, "Fractal design concepts for stretchable electronics," *Nat. Commun.*, vol. 5, pp. 1–8, 2014.

[20] Y. Cho *et al.*, "Engineering the shape and structure of materials by fractal cut," *Proc. Natl. Acad. Sci.*, vol. 111, no. 49, pp. 17390–17395, 2014.

[21] V. Kunin, S. Yang, Y. Cho, P. Deymier, and D. J. Srolovitz, "Static and dynamic elastic properties of fractal-cut materials," *Extrem. Mech. Lett.*, vol. 6, pp. 103–114, 2016.

[22] A. Lendlein and O. E. C. Gould, "Reprogrammable recovery and actuation behaviour of shape-memory polymers," *Nat. Rev. Mater.*, vol. 4, no. 2, pp. 116–133, 2019.

[23] H. W. Huang *et al.*, "Investigation of Magnetotaxis of Reconfigurable Micro-Origami Swimmers with Competitive and Cooperative Anisotropy," *Adv. Funct. Mater.*, vol. 28, no. 36, pp. 1–9, 2018.

[24] L. Jing *et al.*, “Kirigami metamaterials for reconfigurable toroidal circular dichroism,” *NPG Asia Mater.*, vol. 10, no. 9, pp. 888–898, 2018.

[25] A. Oyefusi and J. Chen, “Reprogrammable Chemical 3D Shaping for Origami, Kirigami, and Reconfigurable Molding,” *Angew. Chemie - Int. Ed.*, vol. 56, no. 28, pp. 8250–8253, 2017.

[26] A. Lamoureux, K. Lee, M. Shlian, S. R. Forrest, and M. Shtein, “Dynamic kirigami structures for integrated solar tracking,” *Nat. Commun.*, vol. 6, pp. 1–6, 2015.

[27] Z. Song *et al.*, “Kirigami-based stretchable lithium-ion batteries,” *Sci. Rep.*, vol. 5, no. June, 2015.

[28] Y. Morikawa *et al.*, “Ultrastretchable Kirigami Bioprobes,” *Adv. Healthc. Mater.*, vol. 7, no. 3, pp. 1–10, 2018.

[29] M. A. Dias *et al.*, “Kirigami actuators,” *Soft Matter*, vol. 13, no. 48, pp. 9087–9092, 2017.

[30] G. P. T. Choi, L. H. Dudte, and L. Mahadevan, “Programming shape using kirigami tessellations,” pp. 1–16, 2018.

[31] A. Rafsanjani and K. Bertoldi, “Buckling-Induced Kirigami,” *Phys. Rev. Lett.*, vol. 118, no. 8, pp. 1–11, 2017.

[32] T. C. Shyu *et al.*, “A kirigami approach to engineering elasticity in nanocomposites through patterned defects,” *Nat. Mater.*, vol. 14, no. 8, pp. 785–789, 2015.

[33] L. Li, J. M. Scheiger, and P. A. Levkin, “Design and Applications of Photoresponsive Hydrogels,” *Adv. Mater.*, vol. 1807333, 2019.

[34] H. Deng, C. Zhang, J. W. Su, Y. Xie, C. Zhang, and J. Lin, “Bioinspired multi-responsive soft actuators controlled by laser tailored graphene structures,” *J. Mater. Chem. B*, vol. 6, no. 34, pp. 5415–5423, 2018.

[35] X. Zhang *et al.*, “Optically- and thermally-responsive programmable materials based on carbon nanotube-hydrogel polymer composites,” *Nano Lett.*, vol. 11, no. 8, pp. 3239–3244, 2011.

[36] A. Toncheva *et al.*, “Bilayer solvent and vapor-triggered actuators made of cross-linked polymer architectures via Diels–Alder pathways,” *J. Mater. Chem. B*, vol. 5, no. 28, pp. 5556–5563, 2017.

[37] M. M. Schmauch, S. R. Mishra, B. A. Evans, O. D. Velev, and J. B. Tracy, “Chained Iron Microparticles for Directionally Controlled Actuation of Soft Robots,” *ACS Appl. Mater. Interfaces*, vol. 9, no. 13, pp. 11895–11901, 2017.

[38] X. Zhao, S. A. Chester, H. Yuk, R. Zhao, and Y. Kim, “Printing ferromagnetic domains for untethered fast-transforming soft materials,” *Nature*, vol. 558, no. 7709, pp. 274–279, 2018.

[39] T. Xu, J. Zhang, M. Salehizadeh, O. Onaizah, and E. Diller,

"Millimeter-scale flexible robots with programmable three-dimensional magnetization and motions," *Sci. Robot.*, vol. 4, no. 29, p. eaav4494, 2019.

[40] W. Hu, G. Z. Lum, M. Mastrangeli, and M. Sitti, "Small-scale soft-bodied robot with multimodal locomotion," *Nature*, vol. 554, no. 7690, pp. 81–85, 2018.

[41] H.-W. Huang, F. E. Uslu, P. Katsamba, E. Lauga, M. S. Sakar, and B. J. Nelson, "Adaptive locomotion of artificial microswimmers," *Sci. Adv.*, vol. 5, no. 1, p. eaau1532, 2019.

[42] L. Hu, Q. Zhang, X. Li, and M. J. Serpe, "Stimuli-responsive polymers for sensing and actuation," *Mater. Horizons*, 2019.

[43] J. B. Tracy and T. M. Crawford, "Magnetic field-directed self-assembly of magnetic nanoparticles," *MRS Bull.*, vol. 38, no. 11, pp. 915–920, 2013.

[44] A. Boczkowska and S. F. Awietjan, "Microstructure and Properties of Magnetorheological Elastomers," *Adv. Elastomers-technology, Prop. Appl.*, pp. 147–180, Jun. 2012.

[45] R. Zhao, Y. Kim, S. A. Chester, P. Sharma, and X. Zhao, "Mechanics of hard-magnetic soft materials," *J. Mech. Phys. Solids*, vol. 124, pp. 244–263, 2019.

[46] N. V. S. Vallabani and S. Singh, "Recent advances and future prospects of iron oxide nanoparticles in biomedicine and

diagnostics," *3 Biotech*, vol. 8, no. 6, pp. 1–23, 2018.

[47] J. Dulińska-Litewka, A. Łazarczyk, P. Hałubiec, O. Szafrański, K. Karnas, and A. Karewicz, "Superparamagnetic iron oxide nanoparticles-current and prospective medical applications," *Materials (Basel).*, vol. 12, no. 4, 2019.

[48] R. A. Revia and M. Zhang, "Magnetite nanoparticles for cancer diagnosis, treatment, and treatment monitoring: Recent advances," *Mater. Today*, vol. 19, no. 3, pp. 157–168, 2016.

[49] J. Estelrich, E. Escribano, J. Queralt, and M. A. Busquets, "Iron oxide nanoparticles for magnetically-guided and magnetically-responsive drug delivery," *Int. J. Mol. Sci.*, vol. 16, no. 4, pp. 8070–8101, 2015.

[50] M. Motornov *et al.*, "Field-directed self-assembly with locking nanoparticles," *Nano Lett.*, vol. 12, no. 7, pp. 3814–3820, 2012.

[51] S. R. Mishra, M. D. Dickey, O. D. Velev, and J. B. Tracy, "Selective and directional actuation of elastomer films using chained magnetic nanoparticles," *Nanoscale*, vol. 8, no. 3, pp. 1309–1313, 2016.

[52] R. M. Erb, J. J. Martin, R. Soheilian, C. Pan, and J. R. Barber, "Actuating Soft Matter with Magnetic Torque," *Adv. Funct. Mater.*, vol. 26, no. 22, pp. 3859–3880, 2016.

[53] S. R. Mishra, M. D. Dickey, O. D. Velev, and J. B. Tracy,

"Selective and directional actuation of elastomer films using chained magnetic nanoparticles," *Nanoscale*, vol. 8, no. 3, pp. 1309–1313, 2016.

[54] J. Kim, S. E. Chung, S. E. Choi, H. Lee, J. Kim, and S. Kwon, "Programming magnetic anisotropy in polymeric microactuators," *Nat. Mater.*, vol. 10, no. 10, pp. 747–752, 2011.

[55] 배건희, "산화철 나노 입자 사슬을 이용한 프랙탈 구조 자기 액추에이터의 거동 제어 Motion Control of Fractal Structure Magnetic Actuator Embedded with Chained Iron Oxide Nanoparticles," Seoul National University, 2019.

[56] J. N. Grima and K. E. Evans, "Auxetic behavior from rotating squares," *J. Mater. Sci. Lett.*, vol. 19, no. 17, pp. 1563–1565, 2000.

[57] J. N. Grima, P. S. Farrugia, C. Caruana, R. Gatt, and D. Attard, "Auxetic behaviour from stretching connected squares," *J. Mater. Sci.*, vol. 43, no. 17, pp. 5962–5971, 2008.

초 록

종이 절단, 키리가미및 그것의 모양 전이 기능의 예술은 과학과 기술 설계의 분야에있는 현저한 전진을 보였다. 키리가미패턴은 평면의 기계적 변형이 2 차원 (2D)과 3 차원 (3D) 모두에서 형상 변형을 유도할 수있는 단일 시트의 소재로 만들어진 컷으로 구성됩니다. 이 놀라운 특성으로 인해, 키리가미패턴은 auxetics 및 기계적 metamaterials과 같은 복잡한 소재 속성을 일으킬 수 있습니다 그들은 평면 변형을 받게되면 확장 어디에. 그러나, 키리가미구조의 기계적 변형은 일반적으로 물리적으로 손이나 기계로 수행되며, 따라서 접근이 어려운 작고 좁은 공간에서의 적용을 제한합니다. 이 문제를 해결하기 위해 본 연구에서는 자기장을 외부 자극으로 사용하여 기리 가미 패턴을 원격 제어하는 기법을 제안한다.

이 연구에서, 2D 및 3D에서의 키리 가미 패턴의 원격 제어는 자기 - 엘라스토머 복합체 내에서 자성 나노 입자 (MNP) 체인의 자기 이방성을 프로그래밍함으로써 증명된다. 고려 된 키리가미패턴은 경첩으로 연결된 여러 개의 사각형 단위로 구성됩니다. 다양한 2D 및 3D 형상 변환은 각 사각형 단위 내의 자기 이방성 및 힌지 배치를 변경하여 생성됩니다. 제조 및 실험 절차는 전자석에 의해 생성 된 균일한 자기장 하에서 수행된다. 실험 결과에 따르면 각 정사각형 단위 내에서 MNP 사슬을 평면 내 및 평면 외로 정렬함으로써 2D 및 3D

형상 변환이 달성 될 수 있음을 보여줍니다. 따라서, 자기 이방성 이리가미 패턴을 제어하기 위해 자기장을 사용하는 제안 된 기술의 유효성이 확인되었다. 키리 가미 패턴의 이러한 자유로운 작동은 약물 전달, 의료 패치 및 인공 밸브와 같은 영역에서 유망한 잠재적 응용을 보여줍니다.

주요어 : 키리가미, 소프트 액추에이터, 자기 이방성 프로그래밍, 사슬형 자기 나노 입자, 2D 작동, 3D 작동.

학 번 : 2017-22386

Acknowledgements

I would like to express my sincere appreciation to my advisor, Professor Sang-Koog Kim, for the time and the continuous support throughout my master's degree studies. His guidance, enthusiasm, and patience were invaluable. Without him, this master's thesis would have not been possible.

I would also like to thank my lab members at the Research Center for Spin Dynamics and Spin-Wave Devices (ReC-SDSW) lab, at Seoul National University, specifically, Bosung Kim, Jaehak Yang, Jae-Hyeok Lee, Yongsub Kim, Jaegun Sim, Geonhee Bae, and Inna Yusnila Khairani, for their time in holding discussions, support, and encouragement throughout my studies. Their help was indispensable in the achievements of my research.

Finally, I would like to express my deepest gratitude to my family: my parents and my brother, for their encouragement, dedication, and unconditional love. Their endless support was what made everything possible, which gave me the confidence and the drive to complete my master studies.